2011 50th IEEE Conference on Decision and Control and
European Control Conference (CDC-ECC)
Orlando, FL, USA, December 12-15, 2011

# On 3D Path Following Control of a Ducted-Fan UAV on $\mathsf{SO}(3)$

Venanzio Cichella °, Roberto Naldi °, Vladimir Dobrokhodov †, Isaac Kaminer † and Lorenzo Marconi °

° CASY-DEIS, Università di Bologna, Bologna, 40133, Italy.
† Naval Postgraduate School, Monterey, USA.

*Abstract*— **This article focuses on the problem of computing a control law for a particular class of tail-sitter aircraft able to switch their flight configuration from hover to level flight and vice-versa. We address the problem of steering a ducted-fan UAV along a given path (path following problem) so as to meet spatial constraints. One possible scenario is the situation where a vehicle is required to execute collision-free maneuvers under strict spatial limitations and arrive at his final destination while pointing with a camera to a moving target. Path following control in 3D builds on a nonlinear control strategy that is first derived at the kinematic level using the Special Orthogonal Group ($\mathsf{SO}(3)$) theory.**

## I. Introduction

Recent advances of aerial robotics have seen the employment of unmanned aerial systems in complex operations, such as, in particular, in environments potentially cluttered with obstacles or humans [1], [2], [3]. In all these scenarios, one of the main challenge that the design of control systems has to face, is given by the presence of hard spatial constraints that the system trajectories have to satisfy to avoid, from one side, undesired contacts with the surrounding infrastructures and, on the other, to reach precisely the desired targets. The interest for this kind of control scenarios is also testified by the European project AIRobots [4] in which the potential of unmanned aerial systems in accomplishing operations such as inspections of large infrastructure is investigated.

In this work, motivated by the scenarios described above, we consider the problem of designing a control strategy to allow a prototype of Vertical-Take-Off and Landing (VTOL) aerial vehicle to navigate in a certain environment by following a given geometric path. The considered prototype consists of a small ducted-fan aerial vehicle (see among others [5]) specifically designed to accomplish operations in potentially cluttered environments. The ducted-fan configuration, in particular, is a special class of tail-sitter vehicle [6] characterized by the presence of an annular fuselage, the duct, protecting the propeller. In this way, this kind of aircraft is potentially capable of coming into contact with the surrounding environment in a non destructive way, and then it can be employed in scenarios in which physical interactions between the vehicle and the environments is possible.

In order to address the path following problem, drawing inspiration from [7] and [8], we consider first a nonlinear control strategy, derived using the Special Orthogonal Group ($\mathsf{SO}(3)$) theory, that allows a *virtual vehicle* to approach exponentially the desired geometric path at a certain desired velocity. The main advantage of the *virtual vehicle* approach is that the path following control problem is solved at the kinematic level, indeed reducing the complexity in the control design. The trajectory of the *virtual vehicle* is then employed as a time reference signal for a nonlinear control law specifically designed for the ducted-fan prototype. Interestingly enough, it is shown how the path following approach - see among others [9], [10] - allows to choose the time law, namely the speed of the *virtual vehicle*, in order to robustly maintain the ducted-fan arbitrarily close to the desired geometric path even in the presence of possible uncertainties characterizing the dynamic model of the system.

The remainder of the paper is organized as follows. Section II presents the path following control law for the *virtual vehicle*. In Section III the dynamical model of the ducted-fan prototype and a nonlinear control law for trajectory tracking is presented. Section IV shows the main properties obtained by employing the path following approach for the ducted-fan prototype. Simulations using a detailed nonlinear model of the vehicle are also given in Section V, revealing how the proposed control strategy can be successfully adopted to meet the spatial constraints of certain scenarios. Finally in Section VI some final remarks are postponed.

## II. Path-Following Control of the *Virtual Vehicle*

The path-following problem for the ducted-fan is first solved considering a *virtual vehicle* in order to generate the references for the on-board ducted-fan autopilot. More precisely, in this Section we formulate a control law for the *virtual vehicle* to converge to a virtual target, denoted in the following as *rabbit*, that is moving along a desired geometric path. To characterize the path-following kinematic-error dynamics, we introduce a frame attached to the *virtual vehicle* and a frame attached to the *rabbit*. Next, we define a generalized error vector between these two moving coordinate systems. With this setup, the path following problem consists

This research is framed within the collaborative project AIRobots (Innovative Aerial Service Robots for Remote inspections by contact, ICT 248669) supported by the European Community under the 7th Framework Programme. Corresponding author: Roberto Naldi, email: roberto.naldi@unibo.it. The research is supported in part by projects US-SOCOM, ONR under Contract N00014-11-WX20047, ONR under Contract N00014-05-1-0828, AFOSR under Contract No. FA9550- 05-1-0157, ARO under Contract No. W911NF-06-1-0330, and CO3AUVs of the EU (Grant agreement n. 231378)

of driving this generalized error vector to zero for any given speed profile $v(t)$.

Let $\mathcal{I}$ denote an inertial frame and let $Q$ be the *virtual vehicle* center of mass. Further, let $p_c(\ell) \in \mathbb{R}^3$, with $\ell \in \mathcal{L} \subset \mathbb{R}$, be the path to be followed, parameterized by its path length $\ell$, and $P$ be the center of mass of the *rabbit*.

Let $\mathcal{F}$ be a *parallel transport frame* attached to the point $P$ on the path, and let $T(\ell)$, $N_1(\ell)$ and $N_2(\ell)$ be orthonormal vectors satisfying the frame equations [11], [12]

$$\begin{bmatrix} \frac{dN_1(\ell)}{d\ell} \\ \frac{dN_2(\ell)}{d\ell} \\ \frac{dT(\ell)}{d\ell} \end{bmatrix} = \begin{bmatrix} 0 & 0 & -k_1(\ell) \\ 0 & 0 & -k_2(\ell) \\ k_1(\ell) & k_2(\ell) & 0 \end{bmatrix} \begin{bmatrix} N_1(\ell) \\ N_2(\ell) \\ T(\ell) \end{bmatrix}, \tag{1}$$

where the parameters $k_1(\ell)$ and $k_2(\ell)$ are related to the curvature $\kappa(\ell)$ and torsion $\tau(\ell)$ of the path (see [11] for details). The vector $N_1(\ell)$, $N_2(\ell)$ and $T(\ell)$ define an orthonormal basis for $\mathcal{F}$. The unit vector $T(\ell)$ is aligned with the *rabbit*'s velocity vector at the point determined by $\ell$, while $N_1(\ell)$ and $N_2(\ell)$ define the normal plane perpendicular to $T(\ell)$. They can be used to construct the rotation matrix $R_F^I(\ell) = [N_1(\ell),\ N_2(\ell),\ T(\ell)]$ from $\mathcal{F}$ to $\mathcal{I}$.

Denote by $\omega_{FI}^F$ the angular velocity of $\mathcal{F}$ with respect to $\mathcal{I}$, resolved in $\mathcal{F}$, which is given by

$$\omega_{FI}^F(t) = \begin{bmatrix} -k_2(\ell)\dot{\ell}(t), & k_1(\ell)\dot{\ell}(t) & 0 \end{bmatrix}^T.$$

Also, let

$$p_I(t) = \begin{bmatrix} x_I(t), & y_I(t), & z_I(t) \end{bmatrix}^T$$

be the position of the *virtual vehicle* center of mass $Q$ resolved in $\mathcal{I}$, and let

$$p_F(t) = \begin{bmatrix} x_F(t), & y_F(t), & z_F(t) \end{bmatrix}^T$$

be the difference between $p_I$ and $p_c$ resolved in $\mathcal{F}$. Let $\mathcal{W}$ denote a *velocity frame* with its origin at Q and its $z$-axis aligned with the velocity vector of the *virtual vehicle*. Next, let $R_I^F$ and $R_I^W$ denote the rotation matrices from $\mathcal{I}$ to $\mathcal{F}$ and from $\mathcal{I}$ to $\mathcal{W}$, respectively. In what follows, $v(t)$ is the magnitude of the *virtual vehicle* velocity vector, $p(t)$, $q(t)$ and $r(t)$ are the $x$-, $y$- and $z$-axis components, respectively, of the *virtual vehicle*'s rotational velocity resolved in $\mathcal{W}$ frame.

With the above notation, the *virtual vehicle* kinematic equations can be written as

$$\begin{cases} \dot{p}_I = R_W^I\, v\, e_3 \\ \dot{R}_W^I = R_W^I(\omega_{WI}^W)^\wedge \end{cases} \tag{2}$$

where $\omega_{WI}^W = [p\ q\ r]^T$ and $(\cdot)^\wedge : \mathbb{R}^3 \to so(3)$ denotes the *hat map* [13]. Next we define a desired attitude rotation matrix $R_D$ which will be used to shape the "approach" angles to the path

$$R_D = [b_{1D}\ \ b_{2D}\ \ b_{3D}] \tag{3}$$

$$b_{3D} = \frac{-K_3 p_{F_{xy}} + de_3}{||K_3 p_{F_{xy}} + de_3||}, \tag{4}$$

$$p_{F_{xy}} = \begin{bmatrix} x_F & y_F & 0 \end{bmatrix}^T,$$

$$b_{2D} = \frac{K_3 y_F e_3 + de_2}{||K_3 y_F e_3 + de_2||}$$

in which $d > 0$ is a control parameter and $b_{1D} = b_{2D} \times b_{3D}$. Clearly, by construction $R_D \in \mathsf{SO(3)}$ and $R_D \to I$ as $p_{F_{xy}} \to 0$. Furthermore, when the *virtual vehicle* is far from the desired path, the approach angles become close to $\pi/2$. As the *virtual vehicle* comes closer to the path, the approach angles tend to 0. Straightforward computations[1] yield the path-following kinematic-error dynamics

$$\mathcal{G}_e : \quad \begin{cases} \dot{p}_F = -\dot{\ell}e_3 - (\omega_{FI}^F)^\wedge p_F + \hat{R}ve_3 \\ \dot{\tilde{R}} = \tilde{R}(\tilde{\omega})^\wedge \end{cases} \tag{5}$$

where $\tilde{R} = R_D^T\hat{R}$, $\hat{R} = R_W^F = R_I^F R_W^I$,

$$\tilde{\omega} = \begin{bmatrix} p \\ q \\ r \end{bmatrix} - \hat{R}^T \begin{bmatrix} -k_2(\ell)\dot{\ell} \\ k_1(\ell)\dot{\ell} \\ 0 \end{bmatrix} - \tilde{R}^T\omega_d \tag{6}$$

and

$$(\omega_d)^\wedge = R_D^T\dot{R}_D.$$

The path following kinematic-error dynamics is then a system with state

$$x_{\rm pf}(t) = \begin{bmatrix} p_F^T & ||e_{\tilde{R}}|| \end{bmatrix}^T \tag{7}$$

and inputs

$$u(t) = \begin{bmatrix} p(t), q(t), r(t), \dot{\ell}(t) \end{bmatrix}^T,$$

where

$$e_{\tilde{R}} = \frac{1}{2}(\tilde{R} - \tilde{R}^T)^\vee$$

model the attitude error, with $(\cdot)^\vee : \mathbb{R}^3 \to so(3)$ denoting the inverse of the *hat map* referred to as the *vee map* [13].

Using the formulation above and given a feasible spatially defined path $p_d(\ell)$, we next define the problem of path following for a *virtual vehicle*:

*Definition 1:* Design feedback control laws for the *virtual vehicle*'s angular rates $p(t)$, $q(t)$ and $r(t)$, and rate of progression of the *rabbit* along the path $\dot{\ell}(t)$ such that the kinematic path following generalized error vector $x_{\rm pf}(t)$ defined in (7) converges to a neighborhood of the origin, independently of the temporal assignments of the mission. □

Stated in simple terms, the problem above amounts to designing feedback laws so that the *virtual vehicle* converges to and remains inside a tube centered on the desired path curve assigned to this *virtual target*, for an arbitrary speed profile v(t) .

In order for the following results to hold we consider the following assumption:

*Assumption 1:* There exist $v_{min} > 0$ and $v_{max} > v_{min}$ such that

$$0 < v_{\rm min} \le v(t) \le v_{\rm max}, \qquad \forall\ t \ge 0. \tag{8}$$

□

[1]A detailed derivation of these dynamics can be found in [14, Sec. 8.2].

Also, given arbitrary positive constants $c$, $K_1$, $K_3$ and $d$ let $c_1$ and $c_2$ be positive constants that satisfy the inequalities

$$\sqrt{cc_1} < 1 \tag{9}$$

$$\frac{K_1}{2c_1}\frac{K_3 v_{min}}{c_2\sqrt{d^2 + K_3^2 2cc_2}} > \frac{{v_{max}}^2}{c_2^2(1-cc_1)^2}\,. \tag{10}$$

Moreover, let $K_2$ satisfy:

$$K_2 \geq \frac{K_3 v_{min}}{\sqrt{d^2 + K_3^2 2cc_2}}\,. \tag{11}$$

Let the rate of progression of the point P along the path be governed by

$$\dot{\ell}(t) = K_2 z_F + e_3^T \hat{R} v e_3 \tag{12}$$

Furthermore, suppose the control inputs $p(t)$, $q(t)$ and $r(t)$ are defined as follows:

$$\begin{bmatrix} p \\ q \\ r \end{bmatrix} = K_1 e_{\tilde{R}}^T + \hat{R}^T \begin{bmatrix} -k_2(\ell)\dot{\ell} \\ k_1(\ell)\dot{\ell} \\ 0 \end{bmatrix} + \tilde{R}^T \omega_d \tag{13}$$

Then the control laws defined by equations (12) and (13) stabilize the subsystem $\mathcal{G}_e$ for any $K_1 > 0$ and $K_3 > 0$. A formal statement of this key result is given in the lemma below.

*Lemma 1:* Let the progression of point $P$ along the path be governed by (12). Then, for any $v(t)$ verifying (8), the origin of the kinematic error equations in (5) with the control inputs $p(t)$, $q(t)$ and $r(t)$ defined in (13) is exponentially stable with the domain of attraction

$$\Omega \;=\; \{x_{\rm pf} \;:\; V_{\rm pf}(x) \leq c\}\,, \tag{14}$$

with

$$V_{\rm pf}(x_{\rm pf}) = \frac{1}{4c_1}\|I - \tilde{R}\|^2 + \frac{1}{2c_2} p_F^T p_F \tag{15}$$

where $c$, $c_1$ and $c_2$ were introduced in (9) and (10)

*Proof:* For a proof of this result the reader is referred to [14, Ch. 8, pp. 122–128]. ∎

*Remark 1:* The formulation and proof of this Lemma was motivated by the work reported in [13].

## III. Ducted-fan Dynamics and Low-Level Control

According to [15], in order to derive a mathematical model for the system, the Newton-Euler equations of a rigid body can be used. In particular the dynamical model of the vehicle with respect to the inertial frame $\mathcal{I}$ is described by

$$\begin{array}{rcl} M\ddot{p} & = & Rf^b \\ J\dot{\omega} & = & -(\omega)^\wedge J\omega + w_{\rm P} G\omega + \tau^b \end{array} \tag{16}$$

where $f^b$ and $\tau^b$ represent respectively the vector of forces and torques applied to the vehicle expressed in a body fixed reference frame $\mathcal{B}$, $M$ the vehicle total mass, $J = diag(j_x, j_y, j_z)$ the diagonal inertia matrix, $p = \text{col}(x, y, z)$ the position of the center of mass, $\omega$ the angular velocity expressed in the body frame, $R$ the rotation matrix relating the body frame and the inertial frame (parameterized by means of roll, $\phi$, pitch, $\theta$, and yaw, $\psi$) and $G = (\text{col}(0, 0, I_{rot}))^\wedge$ with $I_{rot}$ the inertia of the propeller with respect to the spin axis. The term $w_{\rm P} G\omega$ in (16) is introduced to model the gyroscopic precession torque effect due to the angular speed $w_{\rm p}$ of the propeller.

The external wrench vector $col(f^b, \tau^b)$ applied to the rigid body can be seen as a nonlinear function of four *control inputs* $u = col(T, a, b, c)$ with $T$ the propeller thrust, $a$, $b$ and $c$ angular deflections of the control vanes which, deviating the air flow coming from the propeller, are used to govern the attitude dynamics of the system and indeed to counteract the motor torque and to project the propeller thrust in a desired direction. Accordingly, as an approximation, the forces and torques can be written as

$$\begin{array}{rcl} f^b & = & -Te_3 + R^T M g e_3 + R^T f_{rd}(\dot{p}) \\ \tau^b & = & A(T)v + B(T) \end{array} \tag{17}$$

with $v = col(a,\, b,\, c)$ and with

$$A(T) = T\begin{bmatrix} 0 & -k_a & 0 \\ k_a & 0 & 0 \\ 0 & 0 & -k_b \end{bmatrix}, B(T) = \begin{bmatrix} 0 \\ 0 \\ N(T) \end{bmatrix}$$

where $N(T) = (k_N/k_T)T$, with $k_N$, $k_T$, $k_a$ and $k_b$ constant parameters. The term $f_{rd}(\dot{p}_I)$ models the so called *ram-drag* aerodynamic disturbance (see for example [16] and [17]) which, for relative low-speed flight, represents the most relevant drag force contribution affecting the system dynamics. The ram drag results from the application of the momentum theory and corresponds to the force that is required to turn the momentum vector of the air massflow through the fan. In the inertial frame, neglecting the presence of wind, it can be approximated as

$$f_{rd}(\dot{p}) = -\lambda_d \begin{bmatrix} \dot{x} & \dot{y} & 0 \end{bmatrix}^T \tag{18}$$

where $\lambda_d$ collects all the aerodynamic coefficients.

### A. Nonlinear Control Law

Goal of the control law proposed in [15] (to which the reader is referred for a detailed description of the control design) is to generate the four control inputs in order to asymptotically track the four desired vertical, lateral, longitudinal and heading time references $x_{\rm r}(t)$, $y_{\rm r}(t)$, $z_{\rm r}(t)$ and $\psi_{\rm r}(t)$. The reference signals are supposed to be known arbitrary time profiles with the only restrictions dictated by the *functional controllability* of the system and by the fulfillment of physical constraints on the control inputs. For this purpose the overall control law has been divided into a vertical controller and a cascade structure for attitude and lateral/longitudinal control; in the latter, the attitude loop plays the role of *inner loop* and the lateral/longitudinal loop of the *outer loop* . In particular the nonlinear lateral/longitudinal control law has been designed by means of *nested saturations* (see [18]). The overall controller is a mixture of feedforward

control terms (synthesized according to the references) and high gain control terms able to obtain asymptotic tracking of the four reference signals in case of perfect knowledge of the aircraft parameters, otherwise practical tracking with a pre-defined asymptotic bound.

*1) Vertical Control Law:* The vertical dynamics of the system are given by (see (16) and (17))

$$M\ddot{z} = -T\Psi(\Theta) + Mg \tag{19}$$

where $\Psi(\Theta) := C_\phi C_\theta$ (having denoted with $\Theta = \text{col}(\phi, \theta)$). In order to decouple the vertical from the attitude dynamics, we consider the following preliminary choice for the input $T$

$$T = \frac{-T' + M(g - \ddot{z}_\text{r})}{C_{\phi_\text{s}} C_{\theta_\text{s}}} \tag{20}$$

in which $C_{\phi_\text{s}} := max\{C_\phi, C_{\bar{\phi}}\}$ and $C_{\theta_\text{s}} := max\{C_\theta, C_{\bar{\theta}}\}$, with $\bar{\phi}$ and $\bar{\theta}$ chosen s.t.

$$\bar{\phi} \in \left( \|\phi_\text{r}(t)\|_\infty, \frac{\pi}{2} \right), \qquad \bar{\theta} \in \left( \|\theta_\text{r}(t)\|_\infty, \frac{\pi}{2} \right) \tag{21}$$

where $T'$ is an auxiliary control input chosen as the PID control law

$$\begin{array}{rcl} T' & = & \xi - k_{p2}(\dot{e}_z + k_{p1} e_z) \\ \dot{\xi} & = & -k_{p2}(\dot{e}_z + k_{p1} e_z) + M\dot{e}_z \end{array} \tag{22}$$

in which $e_z := z - z_\text{r}$ is the vertical tracking error.

*2) Attitude and Lateral/Longitudinal Control Law:* The control of the attitude dynamics is achieved by means of a law of the form $v = A^{-1}(T)\left(\tilde{v} - B(T)\right)$ with

$$\begin{array}{rcl} \tilde{v} & = & -K_P \left( K_D \omega + \left[ \begin{array}{c} \tan\Theta - A(\Theta_\psi)\Theta_\text{out} \\ \psi + K_\psi \eta_\psi \end{array} \right] \right) + \\ & + & K_P K_D \omega_\text{r} + K_P \left[ \begin{array}{c} \tan\Theta_\text{r} \\ \psi_\text{r} \end{array} \right] + \\ & + & J\dot{\omega}_\text{r} + (\omega_\text{r})^\wedge J \omega_\text{r} - w_{P_\text{r}} G \omega_\text{r} \end{array}$$

in which $K_P$, $K_D$ and $K_\psi$ are design parameters, $\Theta_\text{r}$ and $\omega_\text{r}$ are functions of the lateral, longitudinal, vertical and heading references, (obtained using model inversion of system (16)-(18))

$$A(\Theta_\psi) := \left[ \begin{array}{cc} -C_\psi & S_\psi C_\theta / C_\phi \\ S_\psi / C_\theta & C_\psi / C_\phi \end{array} \right],$$

$\eta_\psi$ is an integrator variable governed by $\dot{\eta}_\psi = \psi - \psi_\text{r}$ and $\Theta_\text{out}$ is a residual control input which will be chosen as the following nested-saturation control law

$$\begin{array}{rcl} \Theta_\text{out} & = & \lambda_3 \sigma \left( \dfrac{\hat{K}_3}{\lambda_3} \xi_3 \right) \\ \xi_3 & := & \left[ \begin{array}{cc} \dot{e}_y & \dot{e}_x \end{array} \right]^\text{T} + \lambda_2 \sigma \left( \dfrac{\hat{K}_2}{\lambda_2} \xi_2 \right) \\ \xi_2 & := & \left[ \begin{array}{cc} e_y & e_x \end{array} \right]^\text{T} + \lambda_1 \sigma \left( \dfrac{\hat{K}_1}{\lambda_1} \xi_1 \right) \\ \xi_1 & := & \left[ \begin{array}{cc} \eta_y & \eta_x \end{array} \right]^\text{T} \end{array}$$

where $e_x := x - x_\text{r}$, $e_y := y - y_\text{r}$ and $\eta_y$, $\eta_x$ represent integrator variables governed by $\dot{\eta}_y = e_y$ and $\dot{\eta}_x = e_x$. In the definition of the outer controller, $(\lambda_i, \hat{K}_i)$, $i = 1, 2, 3$, represent design parameters while $\sigma(\cdot)$ is a *saturation function* rigourously defined in [18].

*3) Control Properties:* Let us denote with the subscript $_0$ the nominal values of the parameters in the dynamical model (16)-(18). For the tracking of the four reference signals, according to [15, Propositions 1 and 3], the following asymptotic bounds hold true:

- there exists $r > 0$ such that

$$\lim_{t\to\infty} \sup \|z(t) - z_\text{r}(t)\| \leq r \|\dot{\varrho}\|_\infty \tag{23}$$

  having defined $\varrho(t) := (M - M_0)(g - \ddot{z}_\text{r})$;
- there exists class-K functions $\gamma_n(\cdot)$, $\gamma_d(\cdot)$ and $\gamma_\Delta(\cdot)$ such that

$$\begin{array}{l} \lim_{t\to\infty} \sup \|(x(t) - x_\text{r}(t), y(t) - y_\text{r}(t), \psi(t) - \psi_\text{r}(t))\| \leq \\ \quad \max \left\{ \lim_{t\to\infty} \sup \gamma_n(|\dot{\varrho}(t)|), \lim_{t\to\infty} \sup \gamma_d(\|d(t)\|), \right. \\ \qquad \left. \lim_{t\to\infty} \sup \gamma_\Delta \left( \left\| \dfrac{\Delta_\text{e}(T)(t)}{K_P} \right\| \right) \right\}. \end{array} \tag{24}$$

  where

$$\begin{array}{rcl} d(\dot{x}_\text{r}, \dot{y}_\text{r}) & := & \left( \frac{M\lambda_{d0}}{M_0} - \lambda_d \right) \left[ \begin{array}{c} \dot{y}_\text{r} \\ \dot{x}_\text{r} \end{array} \right] \\ \Delta_\text{e}(T) & := & \Delta(T) + [L(T)J_0 - J]\dot{\omega}_\text{r} + \\ & + & L(T)(\omega_\text{r})^\wedge J_0 \omega_\text{r} - (\omega_\text{r})^\wedge J \omega_\text{r} + \\ & - & L(T) w_P G_0 \omega_\text{r} + w_P G \omega_\text{r}\,. \end{array}$$

Following the definition in [15], it holds that there exists $\bar{\Delta} \in \mathbb{R}_{\geq 0}$ such that

$$\Delta_\text{e}(T) \leq \bar{\Delta} \max_{j\in 1,2,3,\, h\in 1,2} \{x_\text{r}^{(j)},\, y_\text{r}^{(j)},\, \psi_\text{r}^{(h)}\}$$

in which, for some $s \in \mathbb{R}$, $s^{(i)} := d^i s / dt^i$. The value of $\bar{\Delta}$ in the above expression depends on the uncertainties on the system parameters and, in particular, it is equal to zero in the special case in which all the parameters are perfectly known. In this latter case observe that also terms $\varrho(t)$ and $d(t)$ are identically zero, namely asymptotic tracking of the reference signals is achieved.

## IV. Path-Following Control of the Ducted-Fan Aerial Vehicle

Let us assume that the references $x_\text{r}(t)$, $y_\text{r}(t)$ and $z_\text{r}(t)$ for the low level ducted-fan control law are given by the position $p_I(t)$ of the *virtual vehicle* in (2) and that the yaw reference angle $\psi_\text{r}(t)$ is a given reference signal selected by a high level control law. In practice we consider the *virtual vehicle* as a trajectory generator for the ducted-fan in order to steer the position of the real vehicle over the desired geometric path using the proposed path-following approach.

The overall closed loop system is such that the following result holds.

*Lemma 2:* Let be $p_c(\ell)$ the path to be followed, with $\ell \in \mathcal{L} \subset \mathbb{R}$, and $v(t)$ the desired *virtual vehicle* speed satisfying Assumption 1. Assume that, for all $\ell \in \mathcal{L}$ there exist $m_1 > 0$ and $m_2 > 0$ such that

$$\max_{j\in\{0,1,2\}} \left\{ \left| \frac{\partial^j}{\partial \ell^j} \kappa(\ell) \right| \right\} \leq m_1\,, \max_{j\in\{0,1\}} \left\{ \left| \frac{\partial^j}{\partial \ell^j} \tau(\ell) \right| \right\} \leq m_2$$

and that, for all $t \geq 0$, there exists $m_3 > 0$ such that

$$\max_{j\in\{0,1,2,3\}} \left\{ \left| \frac{d^j}{dt^j} v(t) \right| \right\} < m_3 \,.$$

Then the following results hold

- if the system parameters are perfectly known, then the ducted-fan asymptotically follows the *virtual vehicle*, i.e.

$$\lim_{t\to\infty} \sup \|p(t) - p_I(t)\| = 0 \tag{25}$$

- in case of uncertainties on the system parameters, for any $\mu > 0$ there exists $\bar{v}(\mu) > 0$ such that if

$$\max_{j\in\{0,1,2,3\}} \left\{ \left| \frac{d^j}{dt^j} v(t) \right| \right\} \leq \bar{v}(\mu)$$

and

$$\max_{h\in\{1,2\}} \left\{ \left| \frac{d^h}{dt^h} \psi_{\mathrm{r}}(t) \right| \right\} \leq \bar{v}(\mu)$$

then

$$\lim_{t\to\infty} \sup \|p(t) - p_I(t)\| \leq \mu \tag{26}$$

*Proof:* Let us consider the references $x_{\mathrm{r}}(t)$, $y_{\mathrm{r}}(t)$, $z_{\mathrm{r}}(t)$ given by the position $p_I(t)$ of the *virtual vehicle*. As a consequence of Lemma 1, asymptotically the reference signals for the UAV are given by the position of the *rabbit* over the path $p_c(\ell)$, namely, by considering (2), it follows that

$$\dot{p}_I := R_F^I v e_3 \,.$$

By taking the derivative of $\dot{p}_I$, recalling (1), it holds that

$$\max_{j=1,2,3,4} \left\{ |p_I^{(j)}| \right\} \leq \bar{v}(\mu) \bar{K}(m_1, m_2)$$

where $\bar{K}(m_1, m_2)$ is bounded due to the assumptions on the path curvature and torsion. Then the result follows from the asymptotic properties of the nonlinear control law given in (23) and (24). ■

The previous result establish a link between the choice of the velocity for the *virtual vehicle* and the path following performances of the ducted-fan UAV. In particular it is shown how, even in the presence of parametric uncertainties, the position of the ducted-fan can be rendered arbitrary close to the desired path by a proper choice of the *virtual vehicle* speed $v(t)$. Moreover, in the special case in which the system parameters are known, the trajectory of the ducted-fan asymptotically follows the desired path, regardless the choice of the *virtual vehicle* velocity. The result relies only upon some geometric constraints on the curvature and the torsion of the given geometric path. These constraints are required in order for the *virtual vehicle* approach to generate sufficiently smooth time references to be tracked by the low-level control loop.

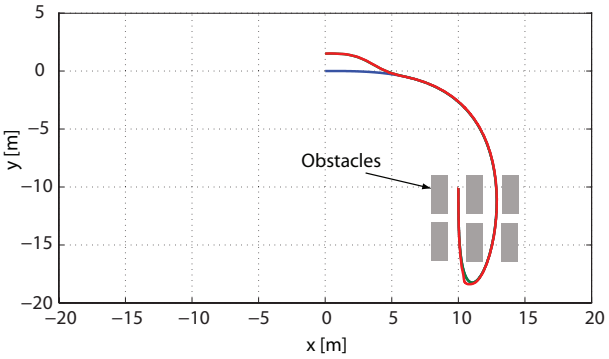


Fig. 1: Path Following ($x$-$y$ plane). $p_c$ (*rabbit*): blue line, $p_I$ (*virtual vehicle*): green line, $p$ (UAV): red line

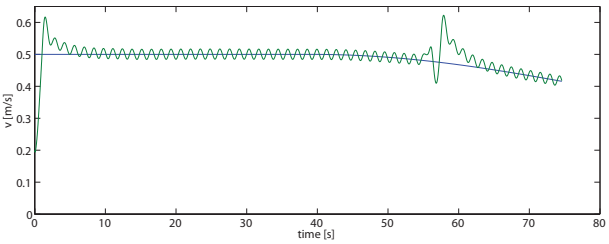


Fig. 2: Velocity error between the *virtual vehicle* and the *rabbit* (blue line) and between the UAV and the *virtual vehicle* (green line)

## V. Simulations

To check the performance of the overall control strategy, a numerical simulation has been implemented. For sake of simplicity in the simulation it has been assumed that the desired yaw reference signal is fixed to zero.

Two different simulations are shown. In the first simulation the UAV has to follow a certain geometric path designed in the $x - y$ inertial 2D plane in order to move the ducted-fan in an environment cluttered with obstacles. The proposed type of geometric path and the given spatial constraints may represent an indoor maneuver or even a motion of the vehicle in an urban canyon. The path and the trajectory obtained by the *virtual vehicle* and the ducted-fan are shown in Figure 1. The velocity of the *virtual vehicle* and of the UAV are depicted in Figure 2. Since in the simulation we assume to have not perfect knowledge of the aerodynamic coefficients in (18), the velocity is kept sufficiently small in order to prevent the real system from impacting the obstacles depicted in Figure 1. The tracking errors along respectively the $x$-, $y$- and $z$-axis are shown respectively in Figure 3.

The second simulation, summarized in Figure 4, demonstrates the capability of the proposed control algorithm to converge to and follow a more aggressive trajectory which evolves also along the vertical axis. The simulation is carried out considering the same parametric uncertainties as in the previous one and assuming the reference yaw angle equal to zero. The *rabbit* starts from initial position $p_c(0) = [0, 0, 0]$ and it ends in position $p_c = [5, 3, 0]$. The UAV starts

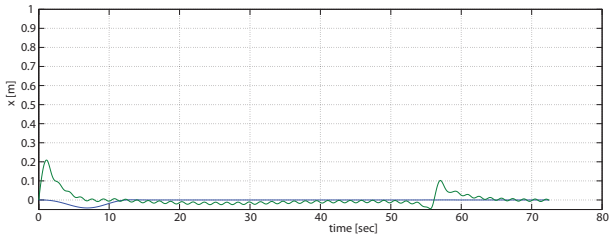


(a) position error along $x$-axis

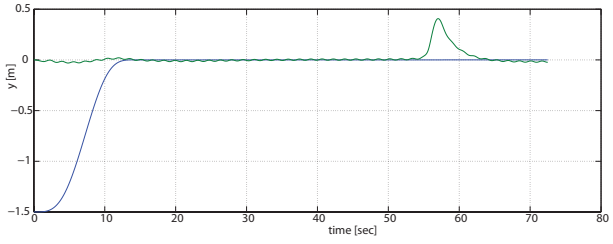


(b) position error along $y$-axis

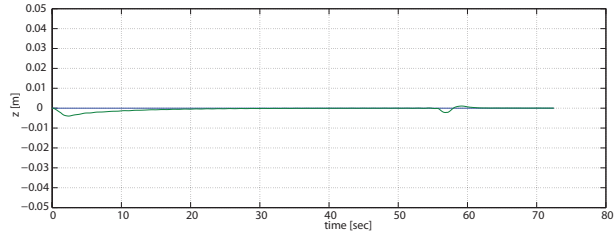


(c) position error along $z$-axis

Fig. 3: Tracking error between the *virtual vehicle* and the *rabbit* (blue line) and between the UAV and the *virtual vehicle* (green line)

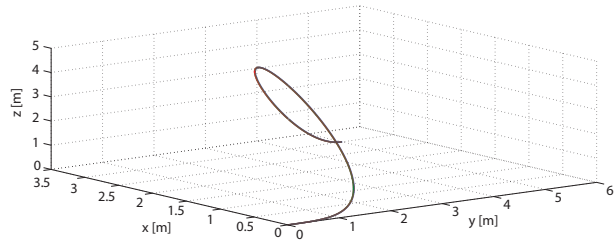


Fig. 4: 3D Path Following. $p_c$ (*rabbit*): blue line, $p_I$ (*virtual vehicle*): green line, $p$ (UAV): red line

following the *rabbit* with no initial error. The velocity $v(t)$ is kept at a constant value given by $0.4\ m/s$. This fact allows to obtain a small tracking error of the *virtual vehicle* trajectory. The geometric path and the trajectory followed by the *virtual vehicle* and the UAV are illustrated in Figure 4.

## VI. Conclusions

In this paper we have considered the problem of steering a ducted-fan aerial robot along a given geometric path in order to meet spatial constraints. A nonlinear control strategy is first derived using the Special Orthogonal Group $(\mathsf{SO}(3))$ theory to allow a *virtual vehicle*, namely a simpler kinematical model, to approach asymptotically the desired geometric path. The trajectory of the *virtual vehicle* is then employed as a reference for a nonlinear control law specifically designed for the ducted-fan prototype. Interestingly enough, it is shown how the path following approach allows to choose the time law, namely the speed of the *rabbit*, in order to robustly, with respect to possible uncertainties in the system parameters, maintain the ducted-fan arbitrarily close to the desired path.

## References


[1] E. Feron and E.N. Johnson. Aerial robotics. In B. Siciliano and O. Khatib, editors, *Springer Handbook of Robotics*, pages 1009–1027. Springer, 2008.

[2] E. Frazzoli, M.A. Dahleh, and E. Feron. Real-time motion planning for agile autonomous vehicles. *AIAA Journal of Guidance, Control, and Dynamics*, 25(1):116–129, 2002.

[3] I.K. Nikolos, K.P Valavanis, N.C. Tsourveloudis, and A.N. Kostaras. Evolutionary algorithm based offline/online path planner for uav navigation. *IEEE Transactions on Systems, Man, and Cybernetics, Part B: Cybernetics*, 33(6):898–912, 2003.

[4] Airobots project website. www.airobots.eu.

[5] O.J. Ohanian III, P.A. Gelhausen, and J. Inman. A compact method for modeling the aerodynamics of ducted fan vehicles. In *Proceedings of the 48th AIAA Aerospace Sciences Meeting Including the New Horizons Forum and Aerospace Exposition*, Orlando,Florida, USA, 2010.

[6] B.W. McCormick. *Aerodynamics of V/STOL flight*. Dover Publications, 1998.

[7] Venanzio Cichella, Enric Xargay, Vladimir Dobrokhodov, Isaac Kaminer, António Pascoal, and Naira Hovakimyan. Geometric 3d path-following control for a fixed-wing uav on $\mathsf{SO}(3)$. In *AIAA Conference of Guidance, Navigation and Control conference*, Portland, OR, August 2011. AIAA-2011-6415.

[8] Isaac Kaminer, António Pascoal, Enric Xargay, Naira Hovakimyan, Chengyu Cao, and Vladimir Dobrokhodov. Path following for unmanned aerial vehicles using $\mathcal{L}_1$ adaptive augmentation of commercial autopilots. *AIAA Journal of Guidance, Control and Dynamics*, 33(2):550–564, March–April 2010.

[9] A.P. Aguiar, J.P. Hespanha, and P. Kokotovic. Path-following for non-minimum phase systems removes performance limitations. *IEEE Transactions on Automatic Control*, (2):234–239, 2005.

[10] R. Skjetne, T.I. Fossen, and P. Kokotovic. Robust output maneuvering for a class of nonlinear systems. *Automatica*, (3):373–383, 2004.

[11] Richard L. Bishop. There is more than one way to frame a curve. *The American Mathematical Monthly*, 82(3):246–251, 1975.

[12] Andrew J. Hanson and Hui Ma. Parallel transport approach to curve framing. Technical report, Indiana University Computer Science Department, 1995.

[13] Melvin Leok Taeyoung Lee and N. Harris McClamroch. Geometric tracking control of a quadrotor uav on $\mathsf{SE}(3)$. In *49th IEEE Conference on Decision and Control*, pages 5420–5425, Atlanta, GA, December 15-17 2010.

[14] Venanzio Cichella. An innovative approach for the uavs path following control and application on a x-3d-bl quadrotor. *DEIS University of Bologna*, 2010. Master Thesis.

[15] R. Naldi, L. Gentili, L. Marconi, and A. Sala. Design and experimental validation of a nonlinear control law for a ducted-fan miniature aerial vehicle. *Control Engineering Practice*, 18(7):747–760, 2010.

[16] A. Ko, O.J. Ohanian, and P. Gelhausen. Ducted fan uav modeling and simulation in preliminary design. In *Proceedings of the AIAA Modeling and Simulation Technologies Conference and Exhibit*, South Carolina, USA, 2007.

[17] E.N. Johnson and M.A. Turbe. Modeling, control, and flight testing of a small ducted fan aircraft. *AIAA Journal of Guidance, Control, and Dynamics*, 29:769–779, 2006.

[18] A. Isidori, L. Marconi, and A. Serrani. *Robust Autonomous Guidance: An Internal Model Approach*. Advances in Industrial Control. Springer-Verlag London, 2003.